Draft version July 27, 2022

Bolometric Luminosity Light Curves and Parameter Estimation for KSP-ZN7090

Patrick Sandoval[1] and Dae-Sik Moon[1,2]

[1] *University of Toronto*
[2] *Department of Astronomy*

1. DISTANCE TO KSP ZN-7090

In the available literature for observed core-collapsed supernovae the quantity used to probe the distance to the object is the luminosity distance. This quantity is the distance to an astronomical source calculated through its intrinsic luminosity, more formally it is defined as the ratio of the bolometric flux to the bolometric luminosity

$$D_L \equiv \sqrt{\frac{L}{4\pi F}} \tag{1}$$

Moreover, using the Robertson-Walker metric and the fact that photons not only decrease in energy but in number density as well at the time of observation we can derive the luminosity distance in terms of the co-moving distance. The co-moving distance is the instantaneous distance between us the and the source.

$$D_L = D_c(1+z) \tag{2}$$

Therefore, in order to find the luminosity distance to ZN7090 we need to know the co-moving distance to the source and the red-shift. A preliminary spectral analysis was carried on ZN-7090's host galaxy and we estimated a red-shift of $z = 0.1$. For the co-moving distance we need to integrate the following expression with respect to redshifts.

$$D_c = \frac{c}{H_0}\int_0^z \frac{dz'}{\sqrt{\Omega_{M,0}(1+z')^3 + \Omega_{k,0}(1+z')^2 + \Omega_{\Lambda,0}}} \tag{3}$$

Where $\Omega_{M,0} = 0.27$ is the present day mass density parameter, $\Omega_{k,0} = 0$ is the curvature density parameter, $\Omega_{\Lambda,0} = 0.73$ is the present day vacuum density parameter, and $H_0 = 74.2\,\mathrm{km/s/Mpc}$ is the present day Hubble constant, all these quantities where taken from Riess et al. 2016. Using these parameters and equations 2 & 3 we compute the luminosity distance to KSP ZN-7090 to be $D_L = 435\,\mathrm{Mpc}$

2. BOLOMETRIC LUMINOSITY LIGHT CURVES

From the results in section 1 we can now compute the absolute bolometric magnitudes and bolometric luminosity from our previous corrections. We begin by applying the distance modulus equation,

$$M = m - 5\log_{10}\left(\frac{D_L}{10\,\mathrm{pc}}\right) \tag{4}$$

and consequently apply the luminosity/flux ratio equation to obtain the bolometric luminosity light curve.

$$\frac{L_{bol,*}}{L_{bol,\odot}} = 100^{(M_{bol,\odot} - M_{bol,*})/5} \tag{5}$$

Where $L_{bol,\odot} = 3.845 \times 10^{33}\,\mathrm{ergs}^{-1}$ and $M_{bol,\odot} = 4.74$ Carroll and Ostlie 2007. Having these equations at hand we can proceed to calculate the bolometric luminosity's for the applied corrections through the same Gaussian sampling method already performed on our previous report.

2.1. *Luminosity Distribution*

From our previous work on adapting the bolometric correction from Martinez et al. 2022 we saw that the distributions for the apparent bolometric magnitude were skewed, which motivated us to use the 50% confidence interval

and the median when graphing the resulting light curve. In this report we have chosen to look at the bolometric corrections provided by Lyman, Bersier, James, et al. 2016 and Lyman, Bersier, and James 2013 because they provide the widest color ranges for our observed colors which improve the confidence of the correction.

Examining the distributions for the bolometric luminosities from the corrections we notice that the distribution for the computed luminosities for the Lyman, Bersier, and James 2013 is moderately skewed, while the distribution for the bolometric luminosities from Lyman, Bersier, James, et al. 2016 are approximately symmetric. We quantify the asymmetry of the distribution by computing the Pearson's median skewness or Pearson's second coefficient of skewness which is defined as follows.

$$\frac{3(\bar{X} - X_{med})}{\sigma} \tag{6}$$

The results of computing said quantity are 0.320, -0.075, and 0.072 for the (B-V), (B-i) and (V-i) corrections respectively, Using the Pearson's media skewness method we are able to quantify the asymmetry of the distribution,

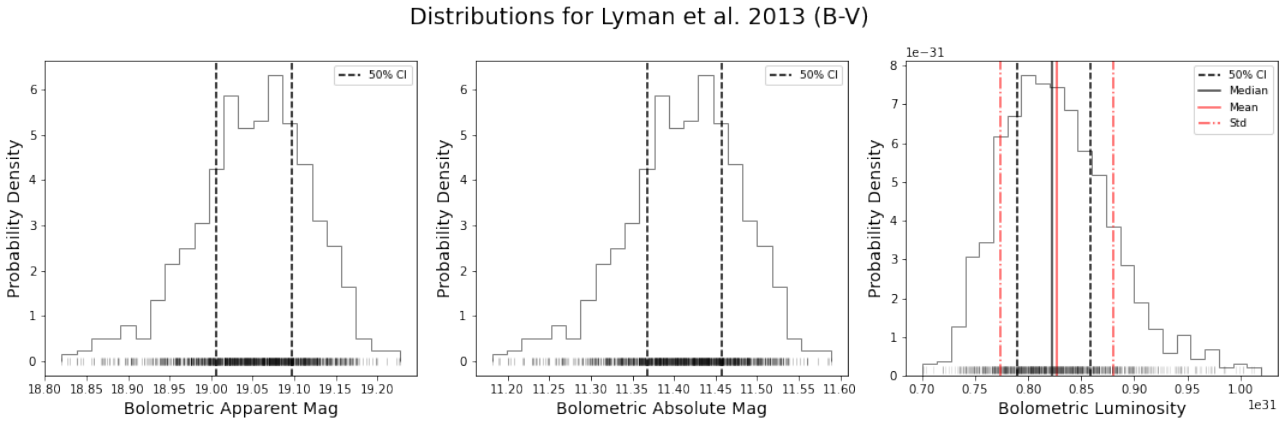

Figure 1: Sample distribution for absolute, apparent bolometric magnitude and bolometric luminosity after adapting the bolometric corrections from Lyman, Bersier, and James 2013 for the color (B-V).

additionally, we will also use quantile-quantile plots to test how well the distribution approximates a theoretical Gaussian. This will help us decide what statistical parameters we should use to properly describe the bolometric luminosity. From all three corrections two distributions from Lyman, Bersier, James, et al. 2016 can be accurately be approximated as Gaussian, meanwhile this approximation breaks for the B-V correction from Lyman, Bersier, and James 2013.

From these results we concluded that we will use the mean and standard deviation to quantify the bolometric luminosities from Lyman, Bersier, James, et al. 2016 and we will the 50% confidence interval and median for the luminosities obtained through the bolometric correction of Lyman, Bersier, and James 2013.

2.2. *Bolometric Light Curves and Optical Light Curves*

As previously mentioned we used a Gaussian sampling method to construct the bolometric light curve for ZN-7090. Furthermore, out all the three corrections used in our previous study we have decided to work with the V-i bolometric correction from Lyman, Bersier, James, et al. 2016 as this correction has the best effective range that covers the highest number of color data points. Additionally the V-i correction had the 2^{nd} tightest correlation following the B-i correction. We believe the most important factor for choosing this bolometric correction is the effective color range as this provides higher confidence to classifying these points as pseudo-bolometric. From Lyman, Bersier, and James 2013 we are told that the filter coverage is from U to K and the color range comes directly from the SNe sample therefore we can approximate the data points within the effective color range as pseudo-bolometric. This allows us to fit the analytical bolometric light curves models to the bolometric data points. Noting the fact that the analytical expression holds only for $T > 0.7\,\mathrm{eV}$ so we would be looking to fit our light curve primarily for these very early hot regions.

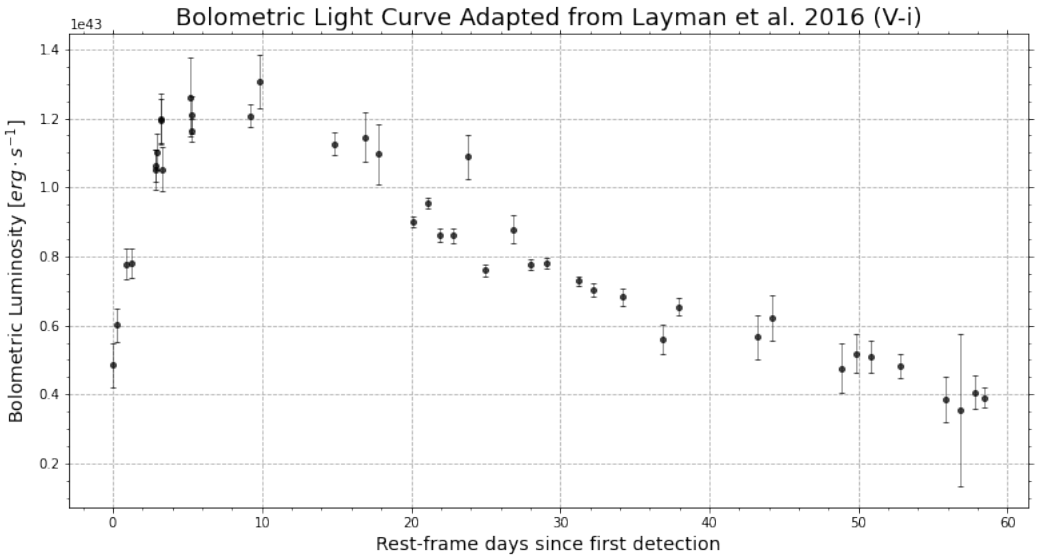

Figure 2: Bolometric light curve adapted from the bolometric correction of Lyman, Bersier, James, et al. 2016 for the (V-i) color. Light curve was constructed through Gaussian sampling on observed magnitudes and applying a bolometric correction to the observed color (V-i), data points represent the mean and standard deviation of the Gaussian sampling.

We see in Figure 3 that the bolometric light curve clearly exhibits the main features of rise and decay in luminosity, as well as a characteristic linear decay post peak. Note that not all the points in Figure 3 are within the effective range therefore, before we fit this bolometric light curve to the analytical models from Sapir and Waxman 2017 and Rabinak and Waxman 2011 we need to remove the data points that are outside the correction's range.

However, a similar result can be obtained by simultaneously fitting the optical light curves of ZN-7090. In order to carry this procedure we need to construct the flux density light curves and to do so we need to recall the definition of the monochromatic magnitude system.

$$m_\lambda = -2.5\log_{10}\left(\frac{f_\lambda}{f_{\lambda,0}}\right) \tag{7}$$

Where f_λ is the flux density per unit wavelength and $f_{\lambda,0}$ is the zero point flux density per unit wavelength specific to each band. For the Vega Johnson-Cousins filters we can find the zero point flux density of each band in table A2 of Bessell, Castelli, and Plez 1998. The corresponding system based in flux per unit frequency is

$$m_\nu = -2.5\log_{10}\left(\frac{f_\nu}{f_{\nu,0}}\right) \tag{8}$$

Where f_ν is the flux density per unit frequency and $f_{\nu,0}$ is the zero point flux density per unit frequency which can be obtained from Table 2a of Fukugita et al. 1996. Lastly we must recall the relationship between f_λ and f_ν

$$f_\lambda = \frac{c}{\lambda^2} f_\nu \tag{9}$$

We can convert the monochromatic apparent magnitude into spectral flux densities per unit wavelength by using the zero point flux density per unit wavelength.

$$f_{\lambda,x} = f_{\lambda_x,0} 10^{-m_x/2.5} \tag{10}$$

However, if we do not know the zero point flux density per unit wavelength we need to know the effective wavelength of the band in order to compute its spectral flux density per unit wavelength.

$$f_{\lambda,x} = \left(\frac{c}{\lambda^2_{eff,x}}\right)(f_{\nu_{eff,x},0})(10^{-m_x/2.5}) \tag{11}$$

With these expressions we are able to construct the flux density light curves for all three optical bands.

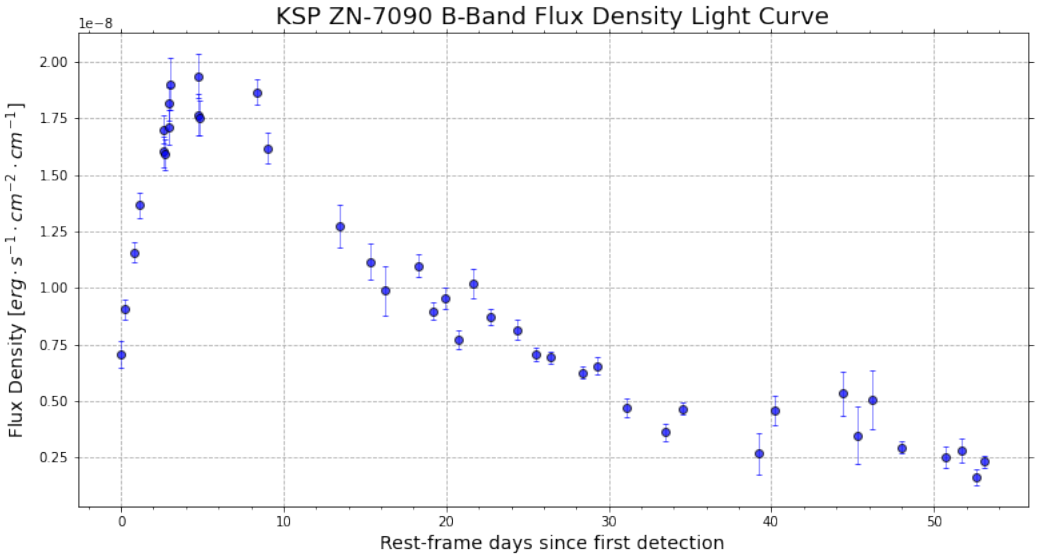

Figure 3: Spectral flux density per unit wavelength light curve for KSP ZN7090 in the Vega Johnson Cousins B-band.

3. PHYSICAL PARAMETERS

To estimate the physical parameters for KSP ZN-7090 we will be performing non-linear fitting on the bolometric light curve for the post peak linear decline and we will also perform simultaneous monochromatic fitting on the optical bands. Consequently we will be comparing the fitting parameters and make a decision as to what approach is more suitable for this task. Rabinak and Waxman 2011 provides analytical expressions for the photospheric temperature and bolometric luminosity for a Type II SN for progenitors with polytropic index of $n = 3/2$ or $n = 3$. The physical difference between these two indices is the type progenitor because an index of $n = 3/2$ indicates a convective effective envelope that corresponds to a red super giant, meanwhile an index of $n = 3$ indicates are radiative effective envelope which corresponds to a blue super giants. Type II CCSNe have strong evidence to have had red super giants as their progenitors, therefore, we will be using all the models corresponding to a polytropic index of $n = 3/2$

$$T_{ph} = 1.6 f_\rho^{-0.037} \frac{E_{51}^{0.027} R_{*,13}^{1/4}}{(M/M_\odot)^{0.054} \kappa_{0.34}^{0.28}} t_5^{-0.45}\,\mathrm{eV} \tag{12}$$

$$L(t) = 8.5 \times 10^{42} \frac{E_{51}^{0.92} R_{*,13}}{f_\rho^{0.27} (M/M_\odot)^{0.84} \kappa_{0.34}^{0.92}} t_5^{-0.16}\,\mathrm{erg\,s^{-1}} \tag{13}$$

We see that Rabinak and Waxman 2011 provides us with analytical expressions for both the bolometric luminosity and the photospheric temperature which gives us two options to conduct the fitting. The first option is to conduct simultaneous monochromatic fitting on the optical light curves to simulate a pseudo-bolometric light curve fit, or we could fit the pseudo-bolometric light curve obtained from applying the bolometric corrections from Lyman, Bersier, James, et al. 2016. However, we must be cautious about this latter approach because we must carefully select which data points can be treated as pseudo-bolometric.

As stated earlier we can derive the theoretical flux density for given temperature and luminosity by noting that spectral flux density per unit wavelength is simply power per unit area per unit frequency. Therefore assuming the

observed source is a black body we recall Planck's law for black-bodies for power per area per frequency per solid angle

$$B_\nu(T) = \frac{2\nu^2}{c^2}\frac{h\nu}{e^{h\nu/kT}-1} \tag{14}$$

Where ν is the frequency of the electromagnetic radiation. From here if we assume that light is emitted isotropically in all direction then we need to perform an integration in spherical coordinates for the polar and azimuthal angles which simplifies to scaling $B_\nu(T)$ by π. This will give is the spectral flux density per unit frequency, however, we are missing one last piece of information and that this the power per unit area given by the Stefan-Boltzmann Law.

$$j^* = \sigma T^4 \tag{15}$$

Taking the ratio of Equation 14 with Equation 15 we get the frequency of the electromagnetic radiation for a specific band. Using this fact we can express the spectral flux density per unit frequency for a specific band as follows.

$$f_{\nu,x} = \frac{\pi B_v(T)}{j^*}\frac{L(t)}{A} \tag{16}$$

Where $L(t)$ is the bolometric luminosity in Equation 13 and $A = 4\pi D_L^2$ is the surface area given by the luminosity distance to ZN-7090. Lastly, in order to fit Equation 16 to Figure 3 we need to use conversion shown in Equation 9 to get the correct units for the fit.

Following these analytical expression we can use the models provided by Rabinak and Waxman 2011 for the photospheric temperature and the bolometric luminosity to simultaneously fit the optical bands.

3.1. *Explosion & Progenitor Parameters*

From the simultaneous monochromatic fitting we extract the ejecta energy and the ejecta mass which are very common parameters presented in SNe observational papers.

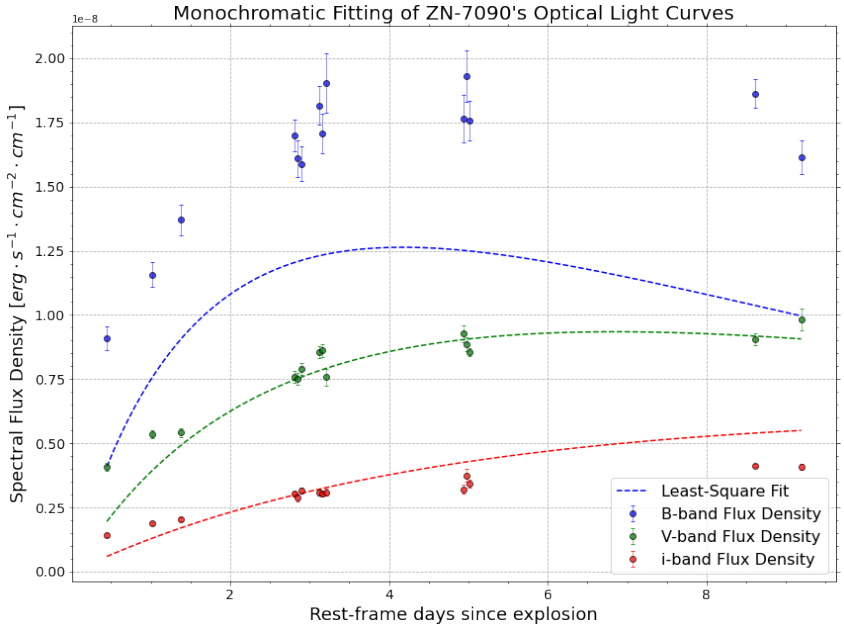

Figure 4: Simultaneous least-square fitting of spectral flux densities per unit wavelength for KSP-ZN7090, adapting analytical solutions for bolometric luminosity and photospheric temperature from Rabinak and Waxman 2011 using Equation 16, with $\chi^2_{red} = 49.60$. The physical parameters extracted by this method include ejecta energy $E_{ej} = 4.08 \times 10^{51}$ erg, ejecta mass $M_{ej} = 10.9\,\mathrm{M}_\odot$ and progenitor radius $R_* = 139\,\mathrm{R}_\odot = 0.967 \times 10^{13}$ cm

The explosion and progenitor parameters are very interesting because we see a fairly energetic explosion for a relative small RSG. We also need to be cautious about the confidence of these values due to the high χ^2_{red}, as we clearly see in Figure 4 that the simultaneous fitting fails to properly fit the blue band light curve. Additionally, Rabinak and Waxman 2011 mentions that in their paper their analytical expressions are only consistent under the constant opacity assumption which is mainly true for the very early hot stage of the SN where the main source of opacity is contributed by Thompson scattering due to the high ionization levels of H in the ejecta. In specific they state their analytical solutions should be used when $T > 0.7\,\mathrm{eV}$, or in an equivalent expression.

$$t < 7.4 \left(\frac{R_{13}}{\kappa_{0.34}} \right)^{0.55} \tag{17}$$

The issue we have for this criteria is that the extent of the fit depends on the parameters of the fit itself, therefore, it becomes ambiguous to determine a proper length for the fit. However, in Figure 18 of Sapir and Waxman 2017 they compare their analytical models to various SNe with known physical parameters and they compare data up until 11 days from the explosion. So in order to have some sort of reference and consistency we also only appliedana their model up until 11 days from the explosion.

Notice that the fitting parameters presented in Figure 4 do not have uncertainties and the reason is because we are not using curve_fit's covariance matrix to estimate such quantities, instead we will look at the contour plots of the reduced chi square for a spectrum of parameters which will help us better understand and constrain these values. We also want to mention that we will be using the distributions of physical parameters for Type II SNe from Martinez et al. 2022 as this paper has been recently published and has a wide range of well studied SNe as its source. From this study we see that the ejecta mass for Type II SNe ranges from $8\,\mathrm{M}_\odot$ to $15\,\mathrm{M}_\odot$. We used this range to provide bounds for curve fit, and from this constrain on the ejecta mass we find the following results about the other two parameters.

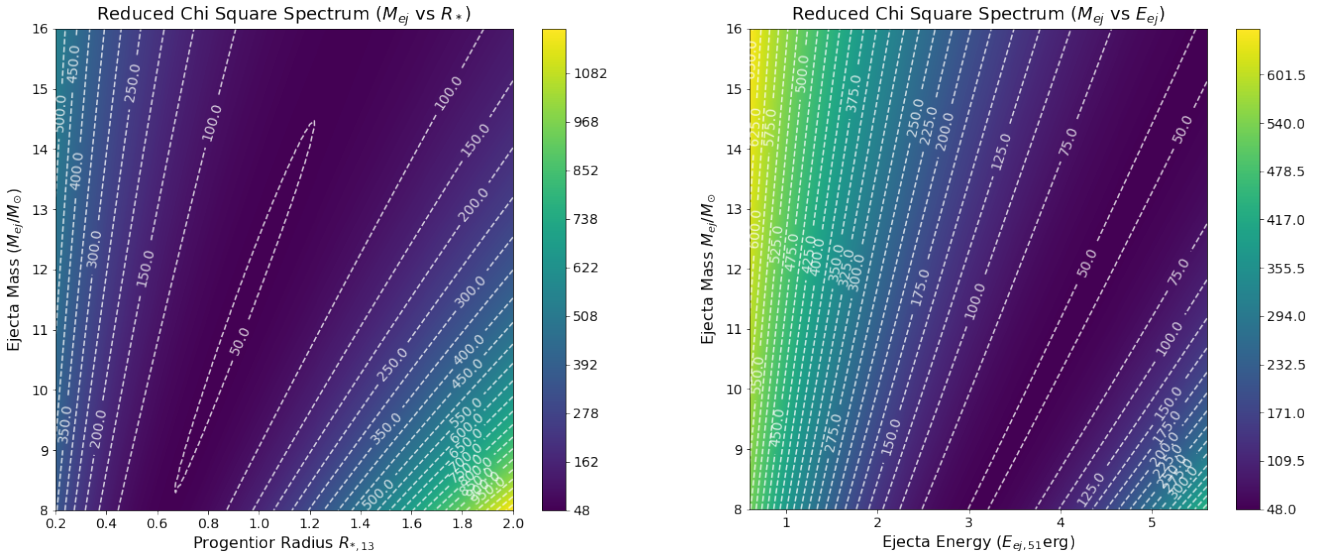

Figure 5: Contour plots for reduced chi squares for combinations of progenitor radius vs ejecta mass (left panel), and ejecta energy vs. ejecta mass (right panel), where the range of the ejecta mass is chosen from distributions of Figure 2 in Martinez et al. 2022

From the contour lines of Figure 5 we can see that in both graphs there are small areas that share the same reduced chi squares, this implies that all those combinations of parameters provide equally good fits, for this reason the uncertainties of each parameter are going to be specified by the range of these areas with same χ^2_{red}. These ranges are $8.12\,\mathrm{M}_\odot \leq M_{ej} \leq 14.47\,\mathrm{M}_\odot$, $0.68\,\mathrm{R}_{*,13} \leq R_{*,13} \leq 1.22\,\mathrm{R}_{*,13}$, and $2.96\,\mathrm{foe} \leq E_{51} \leq 6\,\mathrm{foe}$. By studying the nebular phase of ZN-7090 we can further constrain the ejecta mass and consequently constrain the other two physical

parameters.

However, with a reduced chi square of almost 50 it is too premature to state that we have been able to constrain explosion and progenitor parameters, therefore, we will conduct single band fittings which we believe will have better χ^2_{red}.

Table 1: Explosion and progenitor parameters for multiple bands and single band fits. All fits where provided a bound for the ejecta mass as specified in 3.1

Band/s	E_{ej}	M_{ej}	R_*	χ^2_{red}
	$\times 10^{51}$ erg	$M_\odot$	$\times 10^{13}$ cm	
(B, V, i)	4.06	10.9	0.939	49.60
(B, V)	3.75	10.9	0.772	35.1
(B, i)	3.80	11.0	1.47	60.1
(V, i)	3.54	10.7	0.270	31.43
(B)	3.57	10.8	0.666	6.84
(V)	3.50	10.8	0.241	13.64
(i)	3.44	10.8	0.084	11.62

4. FUTURE STEPS

The the reduced chi squares for all the simultaneous fittings indicates that the model from Rabinak and Waxman 2011 is not applicable to our data, which means we will need to rely on the nebular phase light curve of KSP ZN-7090 to constrain the ejecta mass and consequently use this model again to constrain the progenitor radius. Additionally, we also would want to set the opacity to a constant value instead of fitting it. Additionally, we need to confirm that the early SED of a SN can be treated as a black-body, because the derivation for the theoretical flux density assumes a black-body for the emission.

References

Bessell, M. S., F. Castelli, and B. Plez (May 1998). "Model atmospheres broad-band colors, bolometric corrections and temperature calibrations for O - M stars". In: *A&A* 333, pp. 231–250.

Carroll, Bradley W. and Dale A. Ostlie (2007). *An Introduction to Modern Astrophysics*. Ed. by San Francisco: Pearson Addison-Wesley. 2nd (International).

Fukugita, M. et al. (Apr. 1996). "The Sloan Digital Sky Survey Photometric System". In: *AJ* 111, p. 1748. DOI: 10.1086/117915.

Lyman, J. D., D. Bersier, and P. A. James (Dec. 2013). "Bolometric corrections for optical light curves of core-collapse supernovae". In: *Monthly Notices of the Royal Astronomical Society* 437.4, pp. 3848–3862. ISSN: 0035-8711. DOI: 10.1093/mnras/stt2187. eprint: https://academic.oup.com/mnras/article-pdf/437/4/3848/18500482/stt2187.pdf. URL: https://doi.org/10.1093/mnras/stt2187.

Lyman, J. D., D. Bersier, P. A. James, et al. (Jan. 2016). "Bolometric light curves and explosion parameters of 38 stripped-envelope core-collapse supernovae". In: *Monthly Notices of the Royal Astronomical Society* 457.1, pp. 328–350. DOI: 10.1093/mnras/stv2983. URL: https://doi.org/10.1093%2Fmnras%2Fstv2983.

Martinez, L. et al. (Apr. 2022). "Type II supernovae from the Carnegie Supernova Project-I". In: *Astronomy &amp Astrophysics* 660, A40. DOI: 10.1051/0004-6361/202142075. URL: https://doi.org/10.1051%2F0004-6361%2F202142075.

Rabinak, Itay and Eli Waxman (Jan. 2011). "THE EARLY UV/OPTICAL EMISSION FROM CORE-COLLAPSE SUPERNOVAE". In: *The Astrophysical Journal* 728.1, p. 63. DOI: 10.1088/0004-637x/728/1/63. URL: https://doi.org/10.1088%2F0004-637x%2F728%2F1%2F63.

Riess, Adam G. et al. (July 2016). "A 2.4% DETERMINATION OF THE LOCAL VALUE OF THE HUBBLE CONSTANT". In: *The Astrophysical Journal* 826.1, p. 56. DOI: 10.3847/0004-637x/826/1/56. URL: https://doi.org/10.3847/0004-637x/826/1/56.

Sapir, Nir and Eli Waxman (Apr. 2017). "UV/Optical Emission from the Expanding Envelopes of Type II Supernovae". In: *The Astrophysical Journal* 838.2, p. 130. DOI: 10.3847/1538-4357/aa64df. URL: https://doi.org/10.3847%2F1538-4357%2Faa64df.